Available online at www.sciencedirect.com
ScienceDirect
International Journal of Heat and Mass Transfer 50 (2007) 3447–3460
International Journal of HEAT and MASS TRANSFER
www.elsevier.com/locate/ijhmt

Experimental and numerical studies of liquid flow and heat transfer in microtubes

Zhuo Li, Ya-Ling He, Gui-Hua Tang, Wen-Quan Tao *

School of Energy and Power Engineering, State Key Laboratory of Multiphase Flow, Xi'an Jiaotong University, Xi'an, Shaanxi 710049, PR China

Received 30 May 2005; received in revised form 13 January 2007
Available online 21 March 2007

Abstract

Experimental and numerical studies were conducted to reveal the flow and heat transfer characteristics of liquid laminar flow in microtubes. Both the smooth fused silica and rough stainless steel microtubes were used with the hydraulic diameters of 50–100 μm and 373–1570 μm, respectively. For the stainless steel tubes, the corresponding surface relative roughness was 2.4%, 1.4%, 0.95%. The experiment was conducted with deionized water at the Reynolds number from 20 to 2400. The experimental data revealed that the friction factor was well predicted with conventional theory for the smooth fused silica tubes. For the rough stainless steel tubes, the friction factor was higher than the prediction of the conventional theory, and increased as the surface relative roughness increased. The results also confirmed that the conventional friction prediction was valid for water flow through microtube with a relative surface roughness less than about 1.5%. The experimental results of local Nusselt number distribution along the axial direction of the stainless steel tubes do not accord with the conventional results when Reynolds number is low and the relative thickness of the tube wall is high. The numerical study reveals that the large ratio of wall thickness over tube diameter in low Reynolds number region causes significant axial heat conduction in the tube wall, leading to a non-linear distribution of the fluid temperature along the axial direction. The axial heat conduction effect is gradually weakened with the increase of Reynolds number and the decrease of the relative tube wall thickness and thus the local Nusselt number approaches the conventional theory prediction.

Keywords: Experimental and numerical studies; Surface roughness; Bulk temperature; Axial heat conduction

1. Introduction

The characteristics of flow and heat transfer in microchannels have attracted much attention of researchers because of the rapid developments of microelectromechanical systems (MEMS, [1,2]) and micrototal analysis system (μ-TAS) [3]. These developments have great impacts on the micro electronic cooling techniques [4], the microheat exchanger, bioengineering, human genome project [5,6], medicine engineering, etc. It is evident that the understanding of the microscale phenomena is very important for designing efficient microdevices. To explore the fundamental physical mechanisms of fluid flow and heat transfer in microchannels, many effects, including the size effect, rarefaction effect, surface roughness, viscous effect, electrostatic force effect, axial heat conduction in the channel wall, surface geometry, the measurement errors, etc. should be taken into account. Both experimental and numerical simulation methods have been performed to study the hydrodynamic and heat transfer characteristics of compressible and incompressible fluids in microchannels, and a large number of papers have been published. Divergences of views still exist in quite a few fundamental understandings. In the following only those recent studies related to the liquid flow and or heat transfer in microchannels are reviewed in order of their publication time.

Based on their test results Peng and Peterson [7] proposed two correlations in order to consider the effect of

* Corresponding author. Tel./fax: +86 29 82669106.
E-mail address: wqtao@mail.xjtu.edu.cn (W.-Q. Tao).

0017-9310/$ - see front matter © 2007 Elsevier Ltd. All rights reserved.
doi:10.1016/j.ijheatmasstransfer.2007.01.016

Nomenclature

A	area of the test tube (m^2)
c_p	specific heat of water (J/(kg K))
D	diameter of test tube (μm)
D_h	hydraulic diameter of test tube (μm)
f	friction factor
$f(x_1,\ldots,x_n)$	uncertainty function
h	heat transfer coefficient (W/(m^2 K))
i, j	grid node
I	electric current (A)
k	thermal conductivity (W/(m K))
L	total length of test tube (mm)
L_h	heated length of test tube (mm)
m	mass flow rate of water (kg/s)
M	"axial conduction" number
Nu	Nusselt number
p	pressure (Pa)
p_d	total pressure loss for various factors (Pa)
Δp	pressure drop along test tube (Pa)
Po	Poiseuille number ($Po = f \cdot Re$)
q	heat flux (W/m^2)
Q	heat transfer rate (W)
r	radial coordinate (m)
Re	Reynolds number
R	radius of test tube (μm)
T	temperature (K)
Tw_x	wall temperature along x-direction (K)
ΔT_x	bulk temperature difference along x-direction (K)
u	water velocity along x-direction (m/s)
v	water velocity along radial direction (m/s)
u_m	mean velocity of water (m/s)
U	voltage supply (V)
x	axial coordinate (m)
$x_1,\ldots,x_n$	function variables

Greek symbols

ε	absolute roughness of tube inside surface (μm)
v	kinetic viscosity (m^2/s)
ρ	water density (kg/m^3)
η	dynamic viscosity (Pa s)
Φ	power supply offered by the electrical DC power (W)
$\dot{\Phi}$	heat source in wall (W/m^3)

Subscripts

ave	average
b	bulk temperature
c	cross-section
cond	conduction heat transfer
conv	convective heat transfer
exp	experimentally determined value
i	inner of test tube
in	inlet
int	linear interpolation of numerical results
l	liquid
num	numerically determined value
o	outer of test tube
out	outlet
s	solid
w	wall surface
1,…,5	natural number of thermocouple

the aspect ratio on the flow and heat transfer in microchannels. In both the laminar and in turbulent regime, the Nusselt number was found to be dependent on the Reynolds number, the Prandtl number, the microchannel aspect ratio and the ratio between the hydraulic diameter and the microchannel width. The authors considered that the geometric configuration of the microchannel had a critical effect on the single-phase convective heat transfer.

Mala and Li [8] performed experiment of water flow in circular microtubes of fused silica and stainless steel with the hydraulic diameter ranging from 50 to 254 μm. The mean surface roughness of the tubes was ±1.75 μm and the relative roughness (ε/D_h) was from 1.36% to 1.70% for the tubes with $D_h = 254$ μm and $D_h = 50$ μm, respectively. They observed a nonlinear trend between pressure drop and flow rate for low Reynolds number, and the friction factors were consistently higher than those predicted by conventional correlations. The transition Reynolds number from laminar to turbulent flow was in the range of 300–1500. They attributed it to the effect of the surface roughness of the microtubes.

Qu et al. [9] conducted experiments to investigate flow characteristics of water through trapezoidal silicon microchannels with $D_h = 51$–169 μm and $\varepsilon/D_h = 3.5$–5.7%. The experimental results indicated that flow friction factor was 8–38% higher than those given by the conventional theory. The authors considered that surface roughness effect led to the higher pressure gradient and flow friction. A roughness-viscosity model was proposed in particular to interpret the experimental data.

The role of the surface roughness not only affected the flow characteristics but also broke the velocity boundary layer and led to higher Nusselt numbers. Rahman [10] conducted experimental measurements for pressure drop and convective heat transfer in silicon microchannel heat sinks with water as coolant. The hydraulic diameter was in the range of 299–491 μm. The friction factor of the experimental result was in the same order compared with the conventional prediction. The results of Nusselt numbers showed that the measured values of the average Nusselt number were usually larger than those predicted by the conventional correlations.

To investigate the role of the surface relative roughness effect on pressure drop and heat transfer characteristics in microtubes, Kandlikar et al. [11] performed experiments of water flow in two tubes with different diameters (1067 and 620 μm). The results showed that for the 1067 μm diameter tube, the effects of the relative roughness from 0.178% to 0.3% on pressure drop were insignificant and the tube could be considered smooth. For the 620 μm diameter tube, the same relative roughness value increased the pressure drop; that is to say, the tube of 620 μm with a relative roughness 0.3% cannot be considered as smooth. Furthermore, the experimental results of the heat transfer increased with higher relative roughness especially for the 620 μm tube. For smooth microtubes the local Nusselt numbers were in good agreement with the theoretical correlation in the thermal entry region of fully developed flow.

Using molecular tagging velocimetry technique Maynes and Webb [12] obtained the velocity distribution in a cross-section of the tube with $D_h = 705$ μm. The profiles for $Re = 550$, 700, 1240, 1600 showed excellent agreement with conventional laminar flow theory. When Reynolds number was greater than 2100, the transition occurred. The Po number is equal to 64 for $Re = 550$–2100.

Celata et al. [13] performed an experimental study of the friction factor in a capillary tube with $D_h = 130$ μm by using R114 as the test fluid. The tube relative surface roughness was 2.65%. Experiments indicated that fRe in laminar flow was in good agreement with the conventional theory. The critical Reynolds number ranged from 1880 to 2480. The authors observed that the high relative roughness played an important role on the transition. The experimental Nusselt numbers were lower than the results from the correlation of Hausen for laminar flow and the correlations of Dittus–Boelter, Gnielinski and Adams–Gnielinski for turbulent flow.

Qu and Mudawar [14] experimentally studied the pressure drop of water flowing in a single-phase microchannel heat sink with $D_h = 349$ μm. The pressure drop was in good agreement with that of the conventional theory prediction. The early transition from laminar to turbulent regime was in the range of $Re = 139$–1672. Good agreement was achieved between the experimental heat transfer result and the numerical simulation of three-dimensional conjugate heat transfer computation.

Various fluids including air, water, and liquid refrigerant R-134a were used by Yang et al. [15] to study the flow friction characteristics in smooth microtubes with $D_h = 173$–4010 μm. The test friction factors agreed very well with Poiseuille equation for laminar regime. The laminar-turbulent transition Reynolds number varied from 1200 to 3800 and increased with decreasing tube diameter.

Both smooth microtubes such as glass, silicon and rough stainless steel microtube with $\varepsilon/D_h = 3$–4% were applied by Li et al. [16] to experimentally study the flow characteristics with deionized water. The diameters of glass, silicon and stainless steel tubes were 79.9–166.3 μm, 100.25–205.3 μm and 129.76–179.8 μm, respectively. For the glass and silicon microtubes with the Reynolds number ranging from 350 to 2300, the results showed that the Poiseuille number remained approximately 64 and the transition Reynolds number was in the range of 2000–2300; for the stainless steel microtubes, the Poiseuille number exceeded 64 corresponding to conventional theory by 37% and 15% for tubes with $D_h = 128.76$ μm, 171.8 μm, respectively, and the transition occurred at $Re = 1700$–1900. The authors highlighted that this conclusion was in contradiction with the conventional theory in which the effect of internal wall relative roughness on laminar flow characteristics were ignored for relative roughness lower than 5%.

Wu and Cheng [17] experimentally studied the deionized water flow characteristics in silicon microchannel with triangular and trapezoid cross-sections. The channels surfaces were smooth. The Reynolds number ranged from 1500 to 2000, and the hydraulic diameter is from 25.9 to 291.0 μm. The experimental results confirmed that the Navier–Stokes equations are still valid for the laminar flow of deionized water in smooth microchannel.

In Ref. [18], Wu and Cheng investigated experimentally 13 different trapezoidal silicon microchannels ($D_h = 25.1$–291 μm). They found that the laminar Nusselt number and apparent friction constant increased with the increase of surface roughness and surface hydrophilic. The Nusselt number increased almost linearly with the Reynolds number at low Reynolds number region ($Re < 100$).

Herwig and Hausner [19] also performed the numerical simulation with experiment conditions of [20] and the result of Nusselt number approached 4.36. Guo et al. [21] have reported that the 1-D model for the thermal resistance based on the assumption of no axial heat conduction in the channel wall causes the experiments results for Nusselt number to be less than the standard value. The transition from laminar to turbulent was experimentally studied by Sharp and Adrian [22] for liquids of different polarities of deionized water, 1-propanol and 20% weight of glycerol solution in glass microtubes with the diameter range of 50–247 μm. Applying micro-PIV to measure the velocity fluctuations, the results showed that the transition to turbulence was the same with the macroflow i.e. $Re_c = 1800$–2300.

Lelea et al. [23] investigated experimentally fluid flow of distilled water in stainless steel microtubes with diameters of 100, 300 and 500 μm at $Re = 50$–800. Both the Po number and the local Nusselt number of the experimental results were in good agreement with conventional theories including the entrance region. The experimental results confirmed the validity of using the conventional or classical theories to predict water flow and heat transfer characteristics in microchannels including the entrance effects.

Li et al. [24] emphasized that the thermophysical properties of the liquid can significantly influence both the flow and heat transfer in the microchannel heat sink. The authors used the numerical simulation to investigate the forced convection heat transfer in silicon-based

microchannel (10 mm × 57 μm × 180 μm) heat sink. The bulk liquid temperature varied in a quasi-linear form along the flow direction for high fluid flow rates.

Furthermore, Koo and Kleinstreuer [25] applied the computer simulation to study the viscous dissipation effects with three different working fluids in microtubes and microchannels. The results showed that for microconduits, viscous dissipation was a strong function of the channel aspect ratio, Reynolds number, Eckert number, Prandtl number and conduit hydraulic diameter. Specially, for water flow in a tube with $D_h < 50$ μm, viscous dissipation became significant and should be considered. Tiselj et al. [26] used the CFD to explain the axial heat conduction phenomenon and good agreement between the experimental results and the numerical results was achieved. Consequently, the authors confirmed the validity of using the conventional theory to describe the liquid heat transfer in microchannels.

More recently, Kandlikar et al. [27] studied the roughness effects in a more detailed manner. Specific experiments were conducted for air and water in rectangular ducts with width of 10.03 mm and variable gap between the two principle walls, resulting $D_h = 325$–1819 μm and $Re = 200$–7200 for air and 200–5700 for water. The surfaces of the two principle walls were roughened by sawtooth ridge elements. The experimental results show that the laminar friction factor results are valid for the relative roughness values up to 14%, while for turbulent flow the effect of surface roughness needs to be further studied. The laminar to turbulent transition is also seen to occur at lower Reynolds numbers for increased relative roughness.

Fakheri and Al-Bakhit [28] numerically solved the three dimensional equations in both solid and fluid to investigate the heat conduction in the wall in microchannel heat exchangers. The results indicated that the wall conduction was significant in the convective heat transfer phenomena in microchannels. Therefore, it can be concluded that the axial heat conduction effect should not be neglected for microchannels because the wall thickness can be of the same order of channel diameter.

Lately, the local and average Nusselt numbers in the laminar flow of a Newtonian fluid through rectangular microchannels were numerically investigated by Lee and Garimella [29]. Both the local and average Nusselt number correlations in the thermal entrance region were proposed. Predictions from these correlations were compared very favorably with previous computational and experimental results for conventional channels, as well as with experimental results for microchannel heat sinks. Recently, based on their own test data and a comprehensive review of experimental results provided with surface roughness information, Tang et al. [30] summarized that the surface roughness would cause significant effect on the gas flow characteristics even if the relative roughness is larger than 1%.

From the above review and comparison, it can be found that for liquid flow in smooth microchannels, the friction factor may be considered in agreement with the conventional prediction. For liquid flow in rough microchannnels, most of the literature presenting the surface relative roughness data reports that the friction factor is higher than that of the macroscale channels, and the surface roughness also leads to the earlier transition from laminar to turbulent. However, in this regard, one issue is still open to discuss as what is the relative roughness limitation below or beyond which the channel can be regarded as smooth or rough. For example, in Ref. [11], the authors emphasized that for the tube of $D_h = 1067$ μm, the effects of the relative roughness from 0.178% to 0.3% on the pressure drop were insignificant and the tube could be considered smooth. Therefore, it is worthwhile to investigate under what condition the surface relative roughness effect can be ignored when studying the liquid flow characteristics in microchannel. As for the laminar convective heat transfer in a relative long microctube, following three issues need to be further clarified. First, when the conventional data deduction method is used to reduce the test data for the local heat transfer coefficients, can we still obtain the results which are similar to the ones of conventional-size tube? If not then what is the reason? And at what conditions can we still obtain the results consistent with the conventional-size situation.

This paper is devoted to both experimental and numerical simulation investigations of liquid flow and heat transfer in microchannels to further clarify the above arguments. The experiment was performed for laminar flow with deionized water flowing in microtubes with the inner diameters $D_h = 300$–1570 μm at $Re = 80$–2400. Then, numerical simulations for heat transfer matching the experiment conditions were conducted. The experimental friction factors were compared with the conventional theory, and the experimental local Nusselt numbers were compared with the numerical simulation results. Finally, the effects of surface roughness and the wall heat conduction on microchannel flow and heat transfer were discussed in detail.

2. Experimental setup

Fig. 1 shows the experimental facility. The working fluid was the deionized water contained in the high-pressure tank driven by compressed nitrogen gas. At the two ends of the tested microtube, two sumps were fabricated to connect the tube. Between the high-pressure tank and the beginning sump, a 0.5 μm filter was placed to prevent particles from entering the test tube. The fused silica tubes and stainless steel (1Cr18Ni9Ti) tubes were used, and the dimensions, surface roughness were listed in Tables 1 and 2. A typical cross-section and the tube inside surface photos by a scanning electron microscope (SEM) are shown in Figs. 2 and 3a–c, respectively. By using a light-section microscope, we measured the surface relative roughness. For the flow friction study both the fused silica and stainless steel tubes were used, and only stainless steel tubes were used for the heat transfer study. There were seven T-type thermocouples with

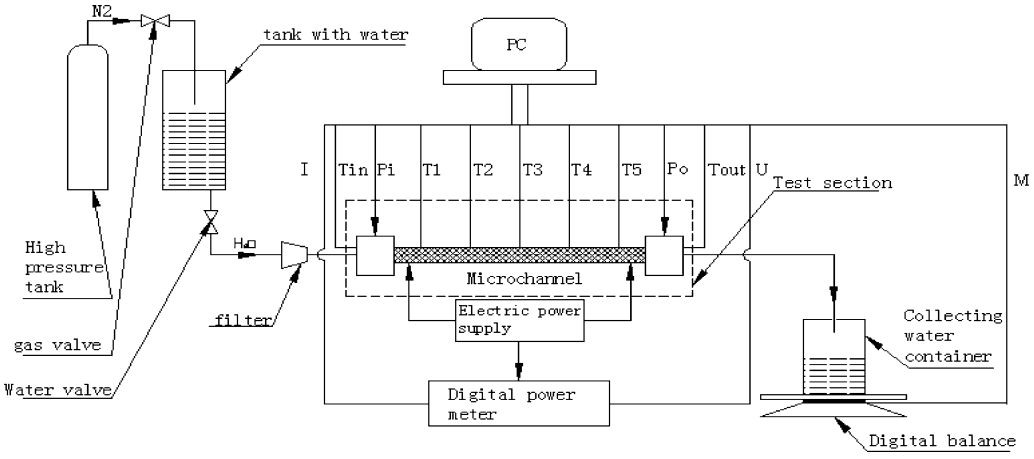

Fig. 1. Schematic diagram of experimental setup.

Table 1
The fused silica test tubes dimensions

Tube	D_i (μm)	L (mm)	ε_{ave} (μm)
No. 1	100	30	≈0
No. 2	75	30	≈0
No. 3	50	30	≈0

the diameter of 50 μm installed at the outside of the tube wall, two placed in the two sumps to measure the inlet and outlet water temperature in the whole experimental process, and the other five were placed on the outside of the tube wall surface along the flow direction to measure the wall temperature in the heat transfer experiment process. A Keithley2700 instrument was used as the data collector in the measurement system.

The heating on the tube wall was offered by an electrical DC power supply (SKD-30V-100A) and a data acquisition logger (HAOO 3D2) was used to measure the input current and voltage. Water flowed through a valve regulator, test section and then was collected by a container. The water container was covered with a glass envelope to avoid evaporation. The water mass flow rate was measured by the water mass collected per unit time on the balance (Sartorius Toploading balance, A-11218-23). The mass flow rate of water was regulated through the gas valve. The pressure drop was measured with the pressure transducer (DP6E22M1B1D) and its outlet was kept at the atmospheric pressure. In the measurement facility, the tube was surrounded with an adiabatic layer composed of mica strap and thermal insulation sponge.

After the test section was assembled, the valve of the pressure tank was opened to drive water into the loop. To ensure single-phase flow in the system, we first boiled the test water to release dissolved gas and then cooled it to the room temperature. Then, the dissolved gas in the whole system was exhausted to the ambient. When the flow rate was stabilized, the DC power supply was turned on to offer the heat source. In general, to reach a steady state needs almost 45 min. All tests were performed under steady-state condition. The thermodynamic properties of deionized water were considered constants by using the mean temperature as the reference temperature. In order to make the figure presentation clear and neat, the arrangements for boiling and cooling the test water to delete gas are not showed in Fig. 1.

3. Experimental data reduction and measurement uncertainty analysis

3.1. Friction factor

The fully developed pressure drop across the microchannels, Δp is obtained [31] by

$$\Delta p = \Delta p_{in,out} - p_d \tag{1}$$

$$p_d = 1.18\rho u_{ave}^2 \tag{2}$$

$$u_{ave} = \frac{m}{\rho A_{c,i}} = \frac{4m}{\rho\pi D_i^2} \tag{3}$$

$$Re = \frac{u_{ave}\cdot D_i}{v} = \frac{4m}{\rho\pi D_i v} \tag{4}$$

$$f = \Delta p\cdot\frac{D_i}{L}\cdot\frac{2}{\rho u_{ave}^2} \tag{5}$$

Table 2
The stainless steel test tubes dimensions

Tube	D_i/D_o (μm)	L (mm)	L_h (mm)	$\frac{D_o-D_i}{2D_i}$	ε_{ave} (μm)	ε_{ave}/D_h (%)	k W/(m K)	Q (W)
No. 4	1570/1810	300	270	7.6	15	0.95	16.3	12
No. 5	624.4/1000	300	270	30	9	1.4		9
No. 6	373/670	300	270	40	9	2.4		9

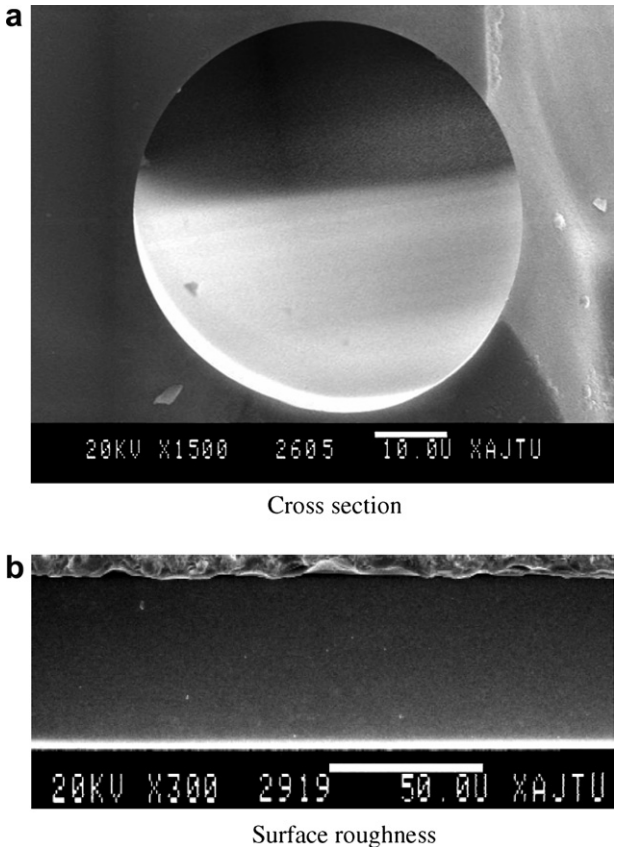

Fig. 2. The SEM images of cross-section and inner surface of typical fused silica test tube with $D_h = 50$ μm.

3.2. Heat transfer

The power supply added to the tube wall can be obtained from Eqs. (6)–(8):

$$\Phi = U \cdot I \tag{6}$$

$$Q = mc_p(T_{out} - T_{in}) \tag{7}$$

$$q = \frac{Q}{A_w} = \frac{mc_p(T_{out} - T_{in})}{\pi D_i L} \tag{8}$$

The local heat transfer coefficient h_x and Nusselt number Nu_x are calculated by the following equations:

$$h_x = \frac{qL_x/L}{\Delta T_x} \tag{9}$$

$$Nu_x = \frac{h_x \cdot D_h}{k_l} = \frac{q \cdot L_x/L \cdot D_h}{\Delta T_x k_l} = \frac{mc_p(T_{out} - T_{in})D_h \cdot L_x/L}{A_w \Delta T_x k_l} \tag{10}$$

$$\Delta T_x = T_{wx} - T_{b,x,int} \tag{11}$$

$$T_{b,x,int} = T_{in} + \frac{Q \cdot L_x/L}{mc_p} \tag{12}$$

In Eq. (11), the inside wall temperature T_{wx} can be obtained from the 1-D heat conduction equation [23]. Although the tube wall temperature distribution is a 2-D function, however, the second derivative of temperature in the axial direction is much less than that in the radial direction, and based on this understanding 1-D heat conduction equation can be used.

As can be seen from Eqs. (10) and (11), to calculate the local heat transfer coefficient and Nusselt number, we must get water bulk temperature $T_{b,x,int}$ distribution along axial direction. It is difficult to measure the fluid bulk temperature directly in the experiment process. For the conventional-size tube, a linear interpolation of the fluid bulk temperature shown by Eq. (12) was adopted, and in this paper we also take the same practice. Special discussion will be given to this practice.

It should be noted here that the heat balance between power supply Φ and the fluid heat transfer rate Q was maintained within 5%.

3.3. Uncertainty analysis

For the experimental study of flow and heat transfer characteristics in microchannel, measurement accuracy is of crucial importance to ensure the validity of the test data. An uncertainty analysis must be performed in order to give some quantitative description of the validity of the test data, even though the analysis results are something uncertain. The uncertainty in determining the friction factor consists of the uncertainties from $\Delta p, D_i, v, M, L$ of Eq. (5). The uncertainty analysis of Nusselt number consists of the uncertainties from $M, c_p, (T_{out} - T_{in}), D_h, L, \Delta T_x, k_l$ of Eq. (10). The analysis of the measurement uncertainty is conducted along the line depicted in [32]. The maximum uncertainties in friction factor and Nusselt number are estimated about 6.6% and 5.5%, respectively. The details of the related parameters uncertainties and the resulted uncertainties in friction factor and Nusselt number are listed in Table 3.

3.4. Numerical simulation

The 2-D Navier–Stokes and energy equations were used to describe the flow and heat transfer in the whole region. Fig. 4 presents the computational domain. The thermal properties were assumed to be constants in the whole region. The following assumptions are adopted: (1) the fluid is incompressible and the fluid flow is in steady state; (2) the flow is laminar; (3) the radiation heat transfer is neglected; (4) the body force is neglected; (5) the electrostatic force is neglected [33,34]; (6) the thermal properties of solid and water are assumed to be constants.

In the axisymmetrical coordinates the governing equations are as follows.

Continuity

$$\rho_l \frac{\partial u}{\partial x} + \rho_l \frac{1}{r} \frac{\partial (r \cdot v)}{\partial r} = 0 \tag{13}$$

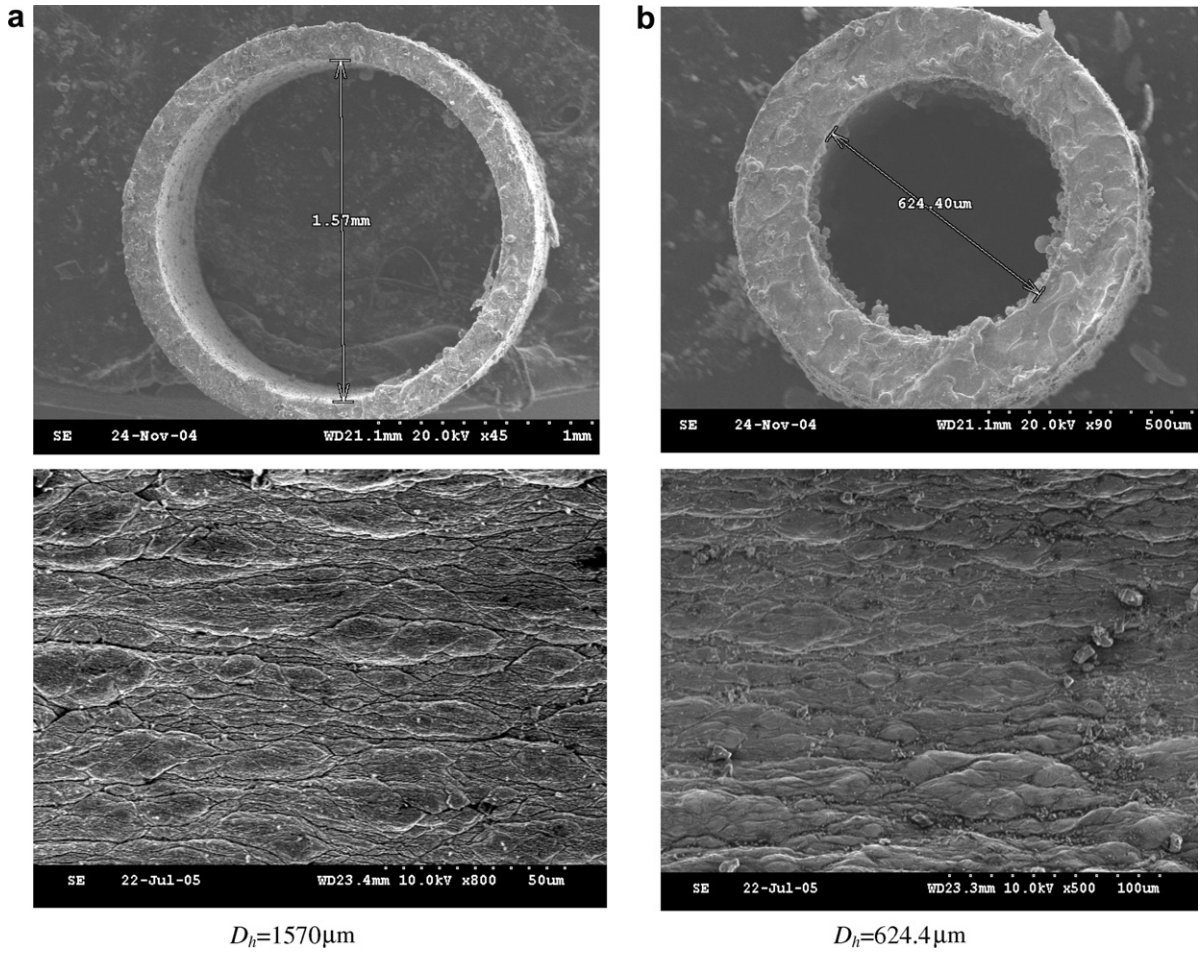

Fig. 3. The SEM images of cross-section and inner surface of three typical stainless steel tested tubes.

Momentum

$$\frac{\partial}{\partial x}(\rho_l uu)+\frac{1}{r}\frac{\partial}{\partial r}(r\rho_l uv)=-\frac{\partial p}{\partial x}+\frac{\partial}{\partial x}\left(\eta_l\frac{\partial u}{\partial x}\right)+\frac{1}{r}\frac{\partial}{\partial r}\left(r\eta_l\frac{\partial u}{\partial r}\right) \tag{14}$$

$$\frac{\partial}{\partial x}(\rho_l uv)+\frac{1}{r}\frac{\partial}{\partial r}(r\rho_l vv)=-\frac{\partial p}{\partial r}+\frac{\partial}{\partial x}\left(\eta_l\frac{\partial v}{\partial x}\right)+\frac{1}{r}\frac{\partial}{\partial r}\left(r\eta_l\frac{\partial v}{\partial r}\right)-\eta_l\left(\frac{v}{r^2}\right) \tag{15}$$

Energy

$$\frac{\partial}{\partial x}(\rho_l c_{p,l} uT)+\frac{1}{r}\frac{\partial}{\partial r}(r\rho_l c_{p,l} vT)=\frac{\partial}{\partial x}\left(k_l\frac{\partial T}{\partial x}\right)+\frac{1}{r}\frac{\partial}{\partial r}\left(rk_l\frac{\partial T}{\partial r}\right)+\dot{\Phi} \tag{16}$$

where $\dot{\Phi}$ is the internal heat source caused by the electrically heating through the tube wall.

The boundary conditions are described as follows.

Because the length of unheated portion of tube is less than 3 mm which is so short compared with the heated potion that can be ignored, and only the heated portion was used in the numerical simulation. At the inlet position, the inlet temperature of liquid is given, and at the domain outlet the flow and heat transfer are assumed to be fully developed:

$$x=0,\quad u=u_{in},\quad v=0,\quad T=T_w=T_{in}$$

$$x=L,\quad \frac{\partial u}{\partial x}=0,\quad \frac{\partial T}{\partial x}=0$$

At the central line

$$0<x<L,\quad r=0,\quad \frac{\partial u}{\partial r}=0,\quad \frac{\partial T}{\partial r}=0,\quad v=0$$

$$\dot{\Phi}=\frac{\Phi}{L_h\cdot\pi(R_o^2-R_i^2)}$$

At outside of the tube wall with insulation:

$$0<x<L,\quad r=R_o,\quad k_s\frac{\partial T}{\partial r}=0$$

In numerical simulation, the local water bulk temperature T_b was defined as follows:

$$T_{b,ave,num}(i)=\frac{\sum_j \rho_l\cdot u(i,j)\cdot c_p\cdot T(i,j)\cdot R(j)\cdot\Delta r}{\sum_j \rho_l\cdot u(i,j)\cdot R(j)\cdot\Delta r\cdot c_p} \tag{17}$$

To numerically determine the local convective heat transfer coefficient, both Fourier's law of heat conduction in the

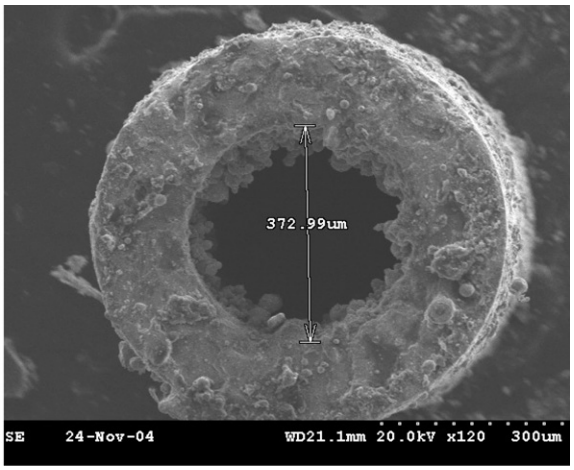

D_h=373μm

Fig. 3 (*continued*)

vicinity of tube inner wall and Newton's law of cooling are used and following equation is adopted:

$$h_x = -\frac{k}{T_{w,x} - T_{b,ave,num}} \left.\frac{\partial T}{\partial r}\right|_{r=R_i} \tag{18}$$

where T_{wx} is the local inner wall surface temperature which can be obtained from numerical computation. For the comparison purpose, the local fluid bulk temperature obtained from linear interpolation of inlet and out fluid temperatures in numerical simulation is also used to numerically determine the local heat transfer coefficient.

Table 3
Measurement uncertainties

Parameters	Maximum uncertainty (%)	Parameters	Maximum uncertainty (%)
D_i	0.6	$\triangle T_x$	3.12
L	0.3	c_p	0.2
$A_{c,i}$	1.2	ρ	0.26
A_w	1.06	v	2
I	0.2	k_l	3
U	0.2	Re	2.43
m	0.2	f	6.56
u_{ave}	0.68	h	4.47
Δp	0.25	Nu	5.48

A special code was developed for the numerical simulation. The finite-volume-method (FVM) [35,36] was used to discretize the governing equations and the SIMPLER algorithm was adopted to deal with the linkage between velocity and pressure. The grid system applied in this paper was 152 (x-direction) × 32 (r-direction). If the relative mass unbalance in the entire domain was less than 10^{-6}, the iteration was terminated. The entire region (include the solid wall) is treated as the computational domain, hence the computation is of conjugated type. The numerical method for such conjugated computation is well documented in Ref. [36], and will not be re-stated here.

4. Results and discussion

4.1. Flow characteristics

According to Eqs. (1)–(5), the experimental friction factors in laminar flow were calculated. As indicated above, the water temperatures at the inlet and the outlet were measured for all experiments and the averaged one was taken as the reference temperature for determining the thermal properties from [37]. For the fused silica tubes experiments were conducted for flow characteristics only and the water

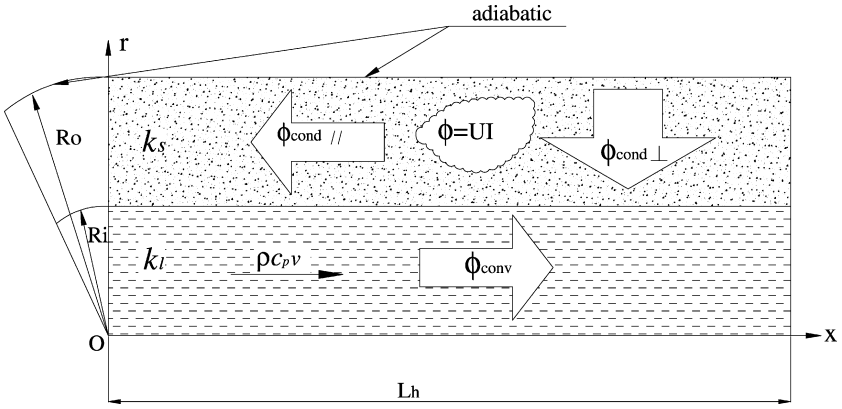

Fig. 4. The computational domain of test tube.

temperature variation was less than 1 °C. The experimental friction factors of the fused silica tubes flow are shown in Fig. 5, and the deviations between the experimental and the conventional results are evaluated and presented in Fig. 6. From Figs. 5 and 6, it can be observed that the experimental friction factors for smooth fused silica test tubes are in good agreement with the prediction of the conventional theory, with almost all the deviations being in the range of ±10%. Furthermore, since the predicted results can be obtained from the Navier–Stokes equations, the results may be regarded as a confirmation that the Navier–Stokes equations are applicable for the water flow in smooth microchannel when the diameter is not less than 50 μm. It should be noted that the ratio of l/d of our test tube is large enough that the effect of the entrance region can be neglected, and the measured pressure drop of the entire tube length can be adopted to obtain the friction factor of the fully developed flow region.

Figs. 7 and 8 show the friction factor and the deviations from the conventional predictions for stainless steel tubes. As seen from Fig. 7, the experimental results of #4 and #5 agree with the conventional theoretical values very well. For conventional-size channels, usually the wall roughness effects on flow characteristics can be neglected if the internal relative roughness is less than 5% [38]. However, for microchannel flow, Tang et al. [30] reported that the surface roughness would cause significant effect on the gas flow characteristics if the relative roughness is larger than 1%. From Fig. 3a–c, it is obvious that with the tube diameter decrease the relative roughness increases. In Table 2, the absolute roughness and the relative roughness are offered, and it can be seen that tube No. 6 has the largest relative roughness. Thus, the larger friction factor of #6 can be attributed to the larger relative roughness and the denser roughness distribution of tube inside. From Fig. 8, it can be observed that when the relative roughness is larger than 1.5%, the friction factor departs from the conventional value and increases gradually, with the deviations being larger than 10%. The results also indicated that the roughness effect can be neglected if the surface relative roughness is less than 1.5% for the deionized water flow in rough microchannel.

From the above results, it can be concluded that for the diameter range, tube material, and working fluid implemented in this study, there exists no non-Stokes phenomenan. The deviation of the measured friction factor from

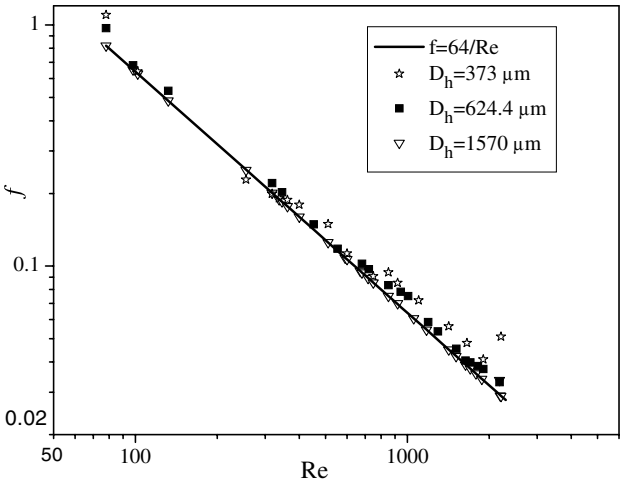

Fig. 7. Friction factors for stainless steel tubes.

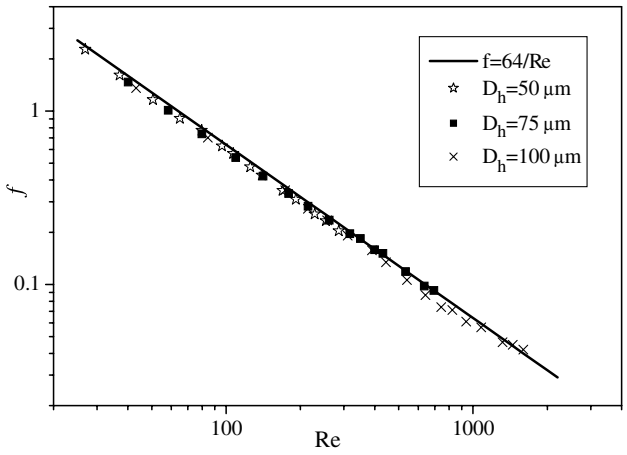

Fig. 5. Measured friction factors for fused silica tubes.

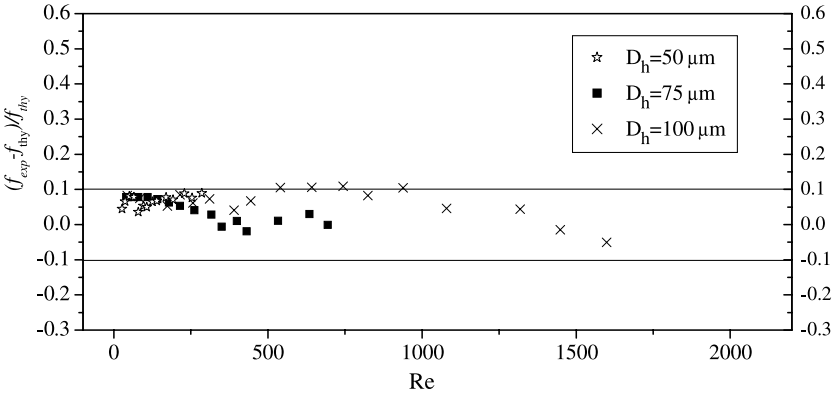

Fig. 6. Deviations between the experimental and the conventional prediction of friction factor for fused silica tubes.

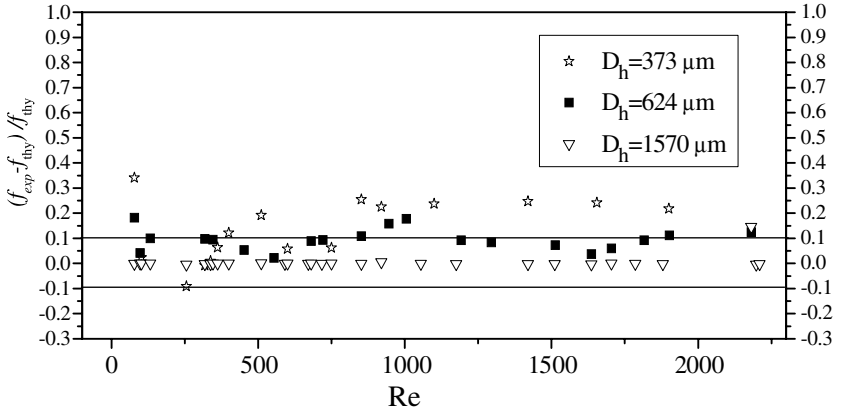

Fig. 8. Deviations between the experimental and the conventional predicted results for stainless steel tubes.

the convectional prediction is caused by the geometric ingredients.

4.2. Heat transfer characteristics

The experimental results and numerical simulation predictions of Nusselt number are presented in Fig. 9a–c. In each figure, there are three curves. They are the numerical simulation result with actual $T_{b,ave,num}$ obtained from Eq. (17) (triangles), numerical simulation result with $T_{b,int,num}$ obtained from linear interpolation between inlet and outlet temperature (circles), and the experimental result with $T_{b,int,exp}$ linearly interpolated from inlet and outlet fluid temperatures of experimental results (closed squares).

Generally speaking, the difference in the determination of T_b leads to different Nusselt number distribution. The ratios of wall thickness to hydrodynamic diameter of tubes #4, #5 and #6 are 0.076, 0.3, and 0.4, respectively. From Fig. 9a–c for test tube #4, it can be seen that the local heat transfer coefficient variation curves do not differ too much, with case of $Re = 80$ being the most. Even for this case the discrepancy between different bulk temperature definitions gradually become smaller and smaller and in the downstream part, three curves coincide with each other quite well. This may imply that the axial heat conduction of tubes #4 does not make significant impact on the convective heat transfer characteristics for the cases studied.

The three curves in Fig. 10a–c of test tube #5 differ from each other more significantly compared with Fig. 9a–c of tube #4. However, the variation trends of these curves also exhibit such a common tendency: the higher the Reynolds number, the smaller the difference, and the local Nusselt number gradually approaches the constant value of 4.36 in the downstream part of the test tube. Such variation tendency can be observed more evidently from Fig. 11a–c of tube #6, which has the largest ratio of tube wall thickness over tube inner diameter.

From above observation of experimental results we may obtain following intuitive conclusions: the larger the tube wall thickness over the tube inner diameter the more significant the tube wall heat conduction; the larger the fluid Reynolds number the weaker the effect of tube wall axial heat conduction and the longer the distance from the tube inlet the smaller the difference of the local Nusselt number from the constant 4.36. This gives us an indication that the effect of the axial heat conduction in the tube wall depends on the relative importance of heat conduction through the tube wall and the convective heat transfer at the tube surface.

To evaluate the heat conduction effect in wall the so-called axial heat conduction number M was introduced in [39], which says

$$M = \frac{\phi_{cond//}}{\phi_{conv}} \tag{19}$$

where $\phi_{cond//}$ is a nominal axial heat conduction with the tube length as its transfer distance and the tube cross-section area as its conduction area, and ϕ_{con} is the convective heat transfer rate determined from enthalpy difference between fluid inlet and outlet. In reference [39] the same temperature difference was used for both tube wall conduction and fluid convection, which is seemingly not physically correct. In this paper the temperature difference in tube wall and in fluids are adopted individually from our numerical simulation results and following calculation equation was used:

$$M = \frac{\phi_{cond//}}{\phi_{conv}} = \frac{A_{c,o} \cdot k_s \cdot \Delta T_s / L_h}{A_{c,i} \cdot \rho c_p \cdot u_{ave} \cdot \Delta T_l} \tag{20}$$

where

$$A_{c,i} = \pi R_i^2 \quad \text{and} \quad A_{c,o} = \pi(R_o^2 - R_i^2) \tag{21}$$

$$\Delta T_l = T_{b,ave,num} - T_{in} \quad \text{and} \quad \Delta T_s = T_{s,out,num} - T_{in} \tag{22}$$

The above-defined non-dimensional number M was used to express the relative importance of the axial heat conduction in the tube wall over the convective heat transfer of the flowing fluid in the tube.

To have a deeper understanding of the effect of tube wall axial heat conduction, special figures of the streamwise variation of the fluid bulk temperature at different Re and M

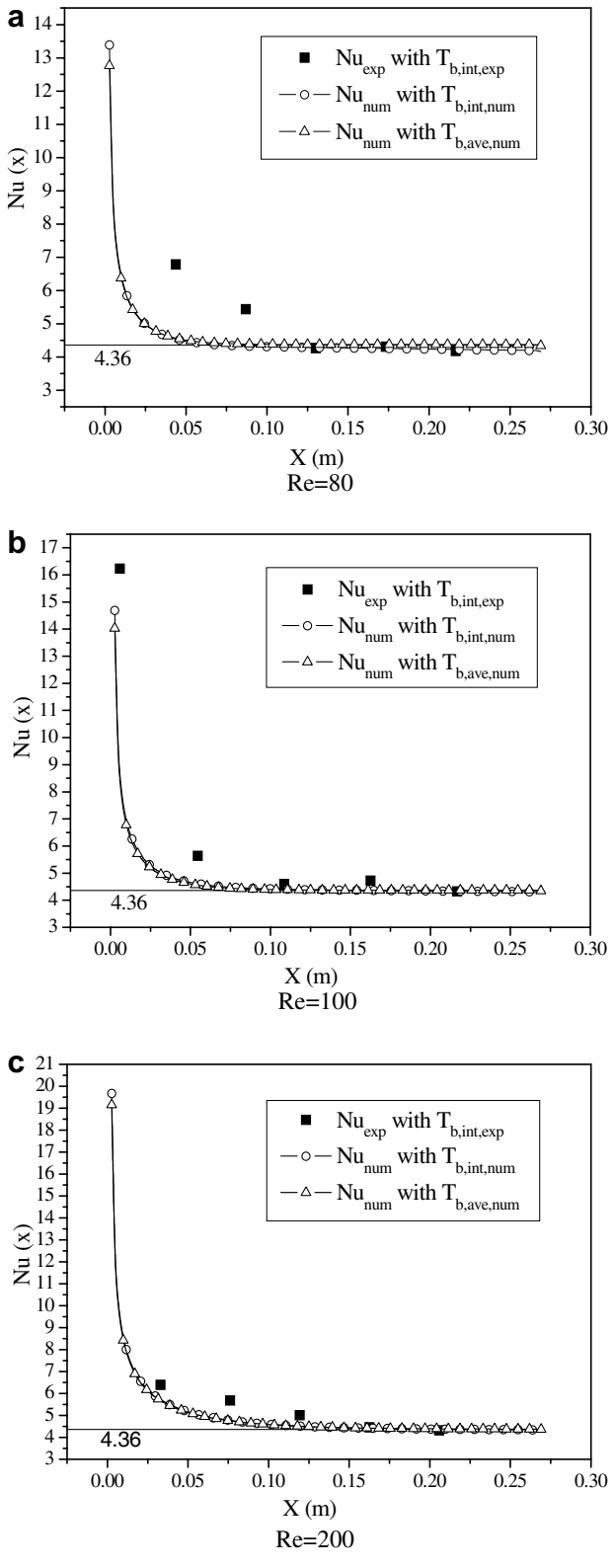

Fig. 9. Local distribution of *Nu* number of tube #4 at different *Re*.

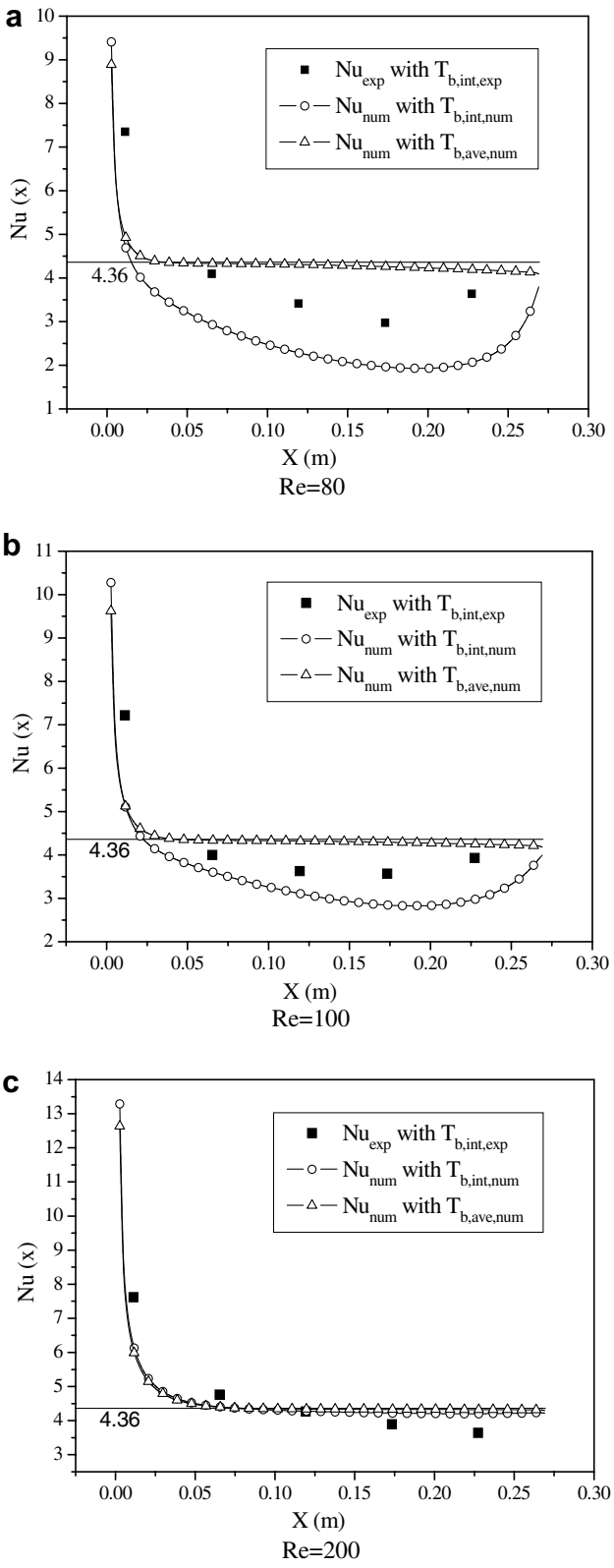

Fig. 10. Local distribution of *Nu* number of tube #5 at different *Re*.

are drawn and shown in Figs. 12–14, where the bulk temperature distributions of numerical simulation for the three stainless steel tubes with the Reynolds number ranging from 80 to 200 are provided. In these figures, the continued lines are the fluid bulk temperature from the linear interpolations, while those symbols are numerically obtained values by Eq. (17). For tube #4 (shown in Fig. 12), the water bulk temperature $T_{b,ave,num}$ distributions

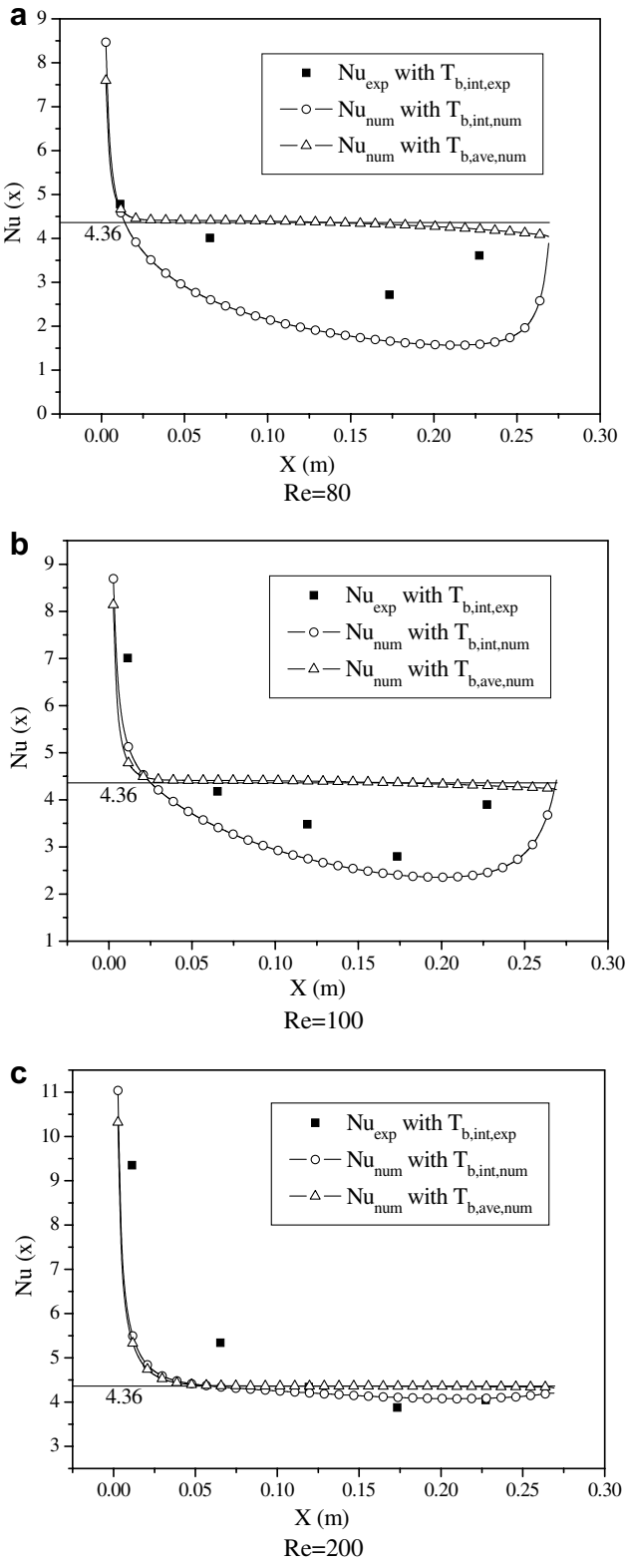

Fig. 11. Local distribution of *Nu* number of tube #6 at different *Re*.

with different Reynolds numbers are in good agreement with the linear interpolation result $T_{b,int,num}$, which indicates that the tube wall axial heat conduction can be neglected and the local Nusselt number can be well predicted by

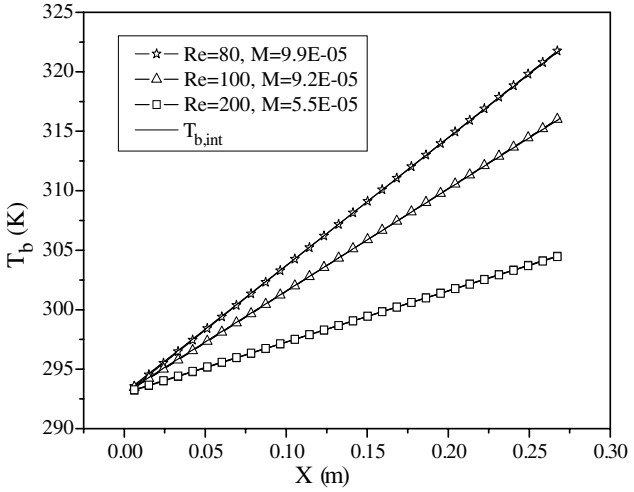

Fig. 12. The bulk temperature distribution and *M* variations with *Re* of tube #4.

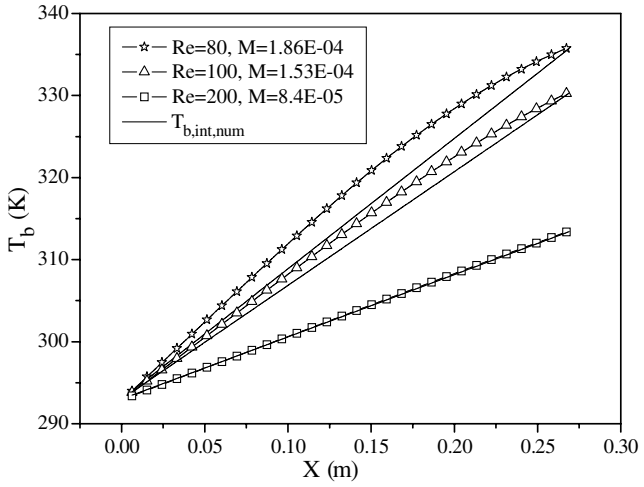

Fig. 13. The bulk temperature distribution and *M* variations with *Re* of tube #5.

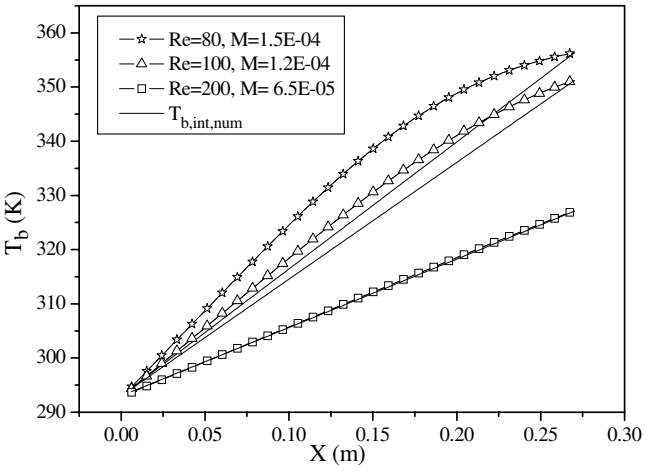

Fig. 14. The bulk temperature distribution and *M* variations with *Re* of tube #6.

the conventional method. For tubes #5 and #6 (shown in Figs. 13 and 14, respectively), it can be seen that for the cases of $Re < 200$ the numerically predicted $T_{b,ave,num}$ distribution departs from $T_{b,int,num}$ appreciably, and the lower the Reynolds number, the larger the departure. This can partly account for what makes the experimental results of the local Nusselt number determined by Eqs. (10) and (11) being different from the conventional theory predictions.

By carefully inspecting Figs. 9–14, it can be observed that for all the cases studied, when the non-dimensional number of M is in the order of 10^{-5}, the interpolated fluid bulk temperature coincides with the one determined by Eq. (17) quite well and the related local Nusselt numbers are in good agreement. This indicates that the tube wall axial heat conduction can be neglected and the conventional data reduction method will lead to expected results. As for the test results, when M is in the order of 10^{-5} (Figs. 10a–c, 10c and 11c) the measured local Nusselt numbers still exhibit some bumpiness around a smooth curve. The present authors believe that this is mainly caused by some inevitable measurement errors of local wall temperatures.

From our numerical practices the present authors realized that whether the tube wall axial heat conduction plays a role depends on quite a few factors, and the value of non-dimensional number M is not the only criterion. From its present definition shown by Eq. (20), it can be found that the denominator is only a nominal axial heat conduction rate, not the actual one. Only when the top and bottom surfaces of the tube wall are adiabatic, the denominator reflects the actual heat conduction in the axial direction. This is one of the reasons why M is not the only criterion for judging whether the axial heat conduction can be neglected. Further study is now underway in the authors' research group and the final results will be reported elsewhere.

In addition, our numerical simulation results show that the major reason that the local heat transfer coefficient deviates from the convectional results comes from two factors: (1) the local heat flux is not equal to the nominal heat flux, and (2) the local fluid bulk temperature is not equal to the linearly interpolated fluid temperature. Both of the two factors are caused by the axial heat conduction in the tube wall. From the authors' knowledge, such detailed analysis has not been presented in the previous literature.

5. Conclusions

In this paper in order to clarify the feasibility of conventional theory to predict the flow and heat transfer characteristics of incompressible fluid flow in microtubes, both experiments and numerical simulation were conducted. The surface roughness effect and the axial heat conduction were the study hot topics. From the results and analysis of the experiment and numerical simulation, the following conclusions are obtained:

(1) The behavior of the deionized water flow in the smooth fused silica microtubes, at least down to $D_h = 50$ μm, shows no differences from macroscale flow. For deionized water flowing through stainless steel microtubes with a relative surface roughness less than about 1.5%, the friction factors also agree well with the conventional theory prediction. When the relative surface roughness is larger than 1.5%, the experimental friction factor of the microtube flow shows an appreciable deviation from the conventional theory.
(2) The experimental local heat transfer results reduced by conventional method in the downstream of tube #5 and #6 show some bias from the conventional results, especially when Reynolds number is low and the relative tube wall thickness is high. The increase of the wall thickness over hydrodynamic diameter ratio leads to a larger discrepancy of heat transfer results between the experimental results reduced by conventional method (or numerical simulation with linear interpolation of the fluid bulk temperature) and conventional result. However, the effect becomes milder with the increase of Reynolds number. After $Re > 100$, with the increase of Reynolds number both the experimental and numerical results gradually approach the conventional heat transfer character. Further research is required in order to clarify under what conditions the tube wall axial heat conduction can be neglected in a general sense.

Acknowledgements

This work is supported by the NNSFC (Nos. 50636050, 50406020) and the National Fundamental R&D Project of China (2007CB206902).

References

[1] C.M. Ho, Y.C. Tai, Micro-electro-mechanical systems (MEMS) and fluid flows, Ann. Rev. Fluid Mech. 30 (1998) 579–612.
[2] M. Gad-el-Hak, The fluid mechanics of microdevices. The Freeman scholar lecture, J. Fluid Eng. 121 (1999) 5–33.
[3] A. Mannz, N. Graber, H.M. Widmer, Miniaturized total chemical analysis systems: a novel concept for chemical sensing, Sensor Actuators B 1 (1990) 244–248.
[4] D.B. Tuckermann, Heat transfer micro-structure for integrated circuits, Ph.D. Thesis, Stanford University, 1984.
[5] K. Kleparnik, Z. Mala, P. Bocek, Fast separation of DNA sequencing fragments in highly alkaline solutions of linear polyacrylamide using electrophoresis in bare silica capillaries, Electrophoresis 22 (2001) 783–788.
[6] W.L. Tseng, H.T. Chang, A new strategy for optimizing sensitivity, speed, and resolution in capillary electrophoretic separation of DNA, Electrophoresis 22 (2001) 763–770.
[7] X.F. Peng, G.P. Peterson, Convective heat transfer and flow friction for water flow in microchannel structures, Int. J. Heat Mass Transfer 39 (1996) 2599–2608.
[8] G.M. Mala, D. Li, Flow characteristics of water in microtubes, Int. J. Heat Fluid flow 20 (1999) 142–148.
[9] W. Qu, Gh.M. Mala, D. Li, Pressure driven water flows in trapezoidal silicon microchannels, Int. J. Heat Mass Transfer 43 (2000) 353–364.

[10] M.M. Rahman, Measurements of heat transfer in microchannel heat sinks, Int. Commun. Heat Mass Transfer 27 (2000) 495–506.
[11] S.G. Kandlikar, S. Joshi, S. Tian, Effect of channel roughness on heat transfer and fluid flow characteristics at low Reynolds numbers in small diameter tubes, in: Proc. of 35th National Heat Transfer Conference, Anaheim CA, USA, 2001, Paper: 12134.
[12] D. Maynes, A.R. Webb, Velocity profile characterization in sub-diameter tubes molecular tagging velocimetry, Exp. Fluids 32 (2002) 3–15.
[13] G.P. Celata, M. Cumo, M. Guglielmi, G. Zummo, Experimental investigation of hydraulic and single phase heat transfer in 0.130 mm capillary tube, Microscale Thermophys. Eng. 6 (2002) 85–97.
[14] W. Qu, I. Mudawar, Experimental and numerical study of pressure drop and heat transfer in a single-phase micro-channel heat sink, Int. J. Heat Mass Transfer 45 (2002) 2549–2565.
[15] C.Y. Yang, J.C. Wu, H.T. Chien, S.R. Lu, Friction characteristics of water, R-134a, and air in small tubes, Microscale Thermophys. Eng. 7 (2003) 335–348.
[16] Z.X. Li, D.X. Du, Z.Y. Guo, Experimental study on flow characteristics of liquid in circular micro-tubes, Microscale Thermophys. Eng. 7 (2003) 253–265.
[17] H.Y. Wu, P. Cheng, Friction factors in smooth trapezoidal silicon microchannels with different aspect ratios, Int. J. Heat Mass Transfer 46 (2003) 2519–2525.
[18] H.Y. Wu, P. Cheng, An experimental study of convective heat transfer in silicon microchannels with different surface conditions, Int. J. Heat Mass Transfer 46 (2003) 2547–2556.
[19] H. Herwig, O. Hausner, Critical view on "new results in micro-fluid mechanics" an example, Int. J. Heat Mass Transfer 46 (2003) 935–937.
[20] C.P. Tso, S.P. Mahulikar, Experimental verification of the role of Brinkman number in microchannels using local parameters, Int. J. Heat Mass Transfer 45 (2002) 2549–2565.
[21] Z.Y. Guo, Z.X. Li, Size effect on microscale single-phase flow and heat transfer, Int. J. Heat Mass Transfer 46 (2003) 149–159.
[22] K.V. Sharp, R.J. Adrian, Transition from laminar to turbulent flow in liquid filled microtubes, Exp. Fluids 36 (2004) 741–747.
[23] D. Lelea, S. Nishio, K. Takano, The experimental research on microtube heat transfer and fluid flow of distilled water, Int. J. Heat Mass Transfer 47 (2004) 2817–2830.
[24] J. Li, G.P. Peterson, P. Cheng, Three-dimensional Φ analysis of heat transfer in a micro-heat sink with single phase flow, Int. J. Heat Mass Transfer 47 (2004) 4215–4231.
[25] J. Koo, C. Kleinstreuer, Viscous dissipation effects in microtubes and microchannels, Int. J. Heat Mass Transfer 47 (2004) 3159–3169.
[26] I. Tiselj, G. Hetsroni, B. Mavko, A. Mosyak, E. Pogrebnyak, Z. Segal, Effect of axial conduction on the heat transfer in microchannels, Int. J. Heat Mass Transfer 47 (2004) 2551–2565.
[27] S.G. Kandlikar, D. Schmitt, A.L. Carrano, J.B. Taylor, Characterization of surface roughness effects on pressure drop in single-phase flow in minichannels, Phys. Fluids 17 (2005) 1–11.
[28] A. Fakheri, H. Al-Bakhit, Entrance and wall conduction effects in parallel flow heat exchangers, in: Proceedings of Fifth International Conference on Enhanced, Compact and Ultra-Compact Heat Exchangers, CHE2005-12, CA., 2005.
[29] P.S. Lee, S.V. Garimella, Thermally developing flow and heat transfer in rectangular microchannels of different aspect ratios, Int. J. Heat Mass Transfer 49 (2006) 3060–3067.
[30] G.H. Tang, Z. Li, Y.L. He, W.Q. Tao, Experimental study of compressibility, roughness and rarefaction influences on microchannel flow, Int. J. Heat Mass Transfer, in press, doi:10.1016/j.ijheatmasstransfer.2006.10.034.
[31] H.B. Ma, G.P. Peterson, Laminar factor in microscale ducts of irregular cross section, Microscale Thermophys. Eng. 1 (1997) 253–265.
[32] R.B. Abernethy, R.P. Benedict, R.B. Dowdell, ASME measurement uncertainty, ASME J. Fluids Eng. 107 (1985) 161–164.
[33] R. Baviere, F. Ayela, Experimental characterization of water flow through smooth rectangular microchannels, Phys. Fluids 17 (2005) 1–4.
[34] Z. Li, G.H. Tang, Y.L. He, W.Q. Tao, Numerical investigation of EDL effects on the flow characteristics of polar fluids in rectangular microchannels, in: Proc. of ASME ICNMM, 2006.
[35] S.V. Patankar, Numerical Heat Transfer and Fluid Flow, Hemisphere, Washington, DC, 1980.
[36] W.Q. Tao, Numerical Heat Transfer, second ed., Xi'an Jiaotong University Press, Xi'an, 2001.
[37] R.C. Weast, M.J. Astle, CRC Handbook of Chemistry and Physics, CRC Press Inc., Boca Raton, FL, 1982.
[38] L.F. Moody, Friction factors for pipe flow, Trans. ASME 66 (1944) 671–684.
[39] G. Maranzana, I. Perry, D. Maillet, Mini- and micro-channels: influence of axial conduction in the walls, Int. J. Heat Mass Transfer 47 (2004) 3993–4004.